LETTER

Contrasting responses of mean and extreme snowfall to climate change

Paul A. O'Gorman[1]

Snowfall is an important element of the climate system, and one that is expected to change in a warming climate[1–4]. Both mean snowfall and the intensity distribution of snowfall are important, with heavy snowfall events having particularly large economic and human impacts[5–7]. Simulations with climate models indicate that annual mean snowfall declines with warming in most regions but increases in regions with very low surface temperatures[3,4]. The response of heavy snowfall events to a changing climate, however, is unclear. Here I show that in simulations with climate models under a scenario of high emissions of greenhouse gases, by the late twenty-first century there are smaller fractional changes in the intensities of daily snowfall extremes than in mean snowfall over many Northern Hemisphere land regions. For example, for monthly climatological temperatures just below freezing and surface elevations below 1,000 metres, the 99.99th percentile of daily snowfall decreases by 8% in the multimodel median, compared to a 65% reduction in mean snowfall. Both mean and extreme snowfall must decrease for a sufficiently large warming, but the climatological temperature above which snowfall extremes decrease with warming in the simulations is as high as −9 °C, compared to −14 °C for mean snowfall. These results are supported by a physically based theory that is consistent with the observed rain–snow transition. According to the theory, snowfall extremes occur near an optimal temperature that is insensitive to climate warming, and this results in smaller fractional changes for higher percentiles of daily snowfall. The simulated changes in snowfall that I find would influence surface snow and its hazards; these changes also suggest that it may be difficult to detect a regional climate-change signal in snowfall extremes.

Extremes of daily precipitation (including liquid and solid precipitation) are found to increase in intensity with climate warming in observations and simulations[8–10], and this is physically consistent with greater saturation-specific humidities in a warmer atmosphere[11–13]. However, little is known about the physical basis for changes in daily snowfall extremes, their past changes on a global or hemispheric scale, or how they change in global-climate-model simulations. Regional observational studies show large interdecadal variations in measures of snowfall extremes[14,15], but long-term trends remain unclear. Extremes of seasonal mean snowfall have been studied previously[16,17], but daily snowfall extremes may respond differently[14]. Physically, we would expect heavy snowfall events to occur in a relatively narrow range of temperatures below the rain–snow transition; at much lower temperatures it is not 'too cold to snow' but low saturation-specific humidities make heavy snowfall unlikely. However, it is not clear what this means for the response to climate change, and previous studies have differed in their findings as to whether heavy snowfall events are predominantly associated with anomalously cold or warm years (or seasons) in the present climate[14,18]. Variability of daily temperatures is another factor that must be taken into account, and cold extremes are expected to persist to some extent in a warming climate[19].

I show here, using simulations and a physically based theory, that snowfall extremes respond more weakly to climate warming than does mean snowfall in many regions. The simulations were performed with 20 climate models and were taken from the World Climate Research Programme's Coupled Model Intercomparison Project phase 5 (CMIP5), which is the first phase of the project to archive daily snowfall (Methods). Climate change was calculated as the difference between the historical simulations (1981–2000; the control climate) and the representative concentration pathway (RCP) 8.5 simulations (2081–2100; the warm climate). The snowfall variable is accumulated daily, includes all solid precipitation at the surface and is expressed in liquid-water equivalent per day (extremes of snowfall depth are discussed in the Methods). For simplicity, only Northern Hemisphere land was considered, and results are presented as the multimodel median of the ratio of snowfall rates in the warm versus the control climate.

Daily snowfall extremes were first measured by their 20-year return values, calculated by fitting the generalized extreme value distribution to the time series of annual maximum daily snowfall in each grid box (Methods). Compared to observational estimates of snowfall, the control simulations capture the magnitudes and many of the features of mean and extreme snowfall, with some regional biases (Extended Data Figs 1 and 2). Climate warming in the simulations causes widespread decreases in mean snowfall at middle latitudes (Fig. 1a), consistent with previous studies[3,4]. In contrast, the snowfall extremes have a relatively muted
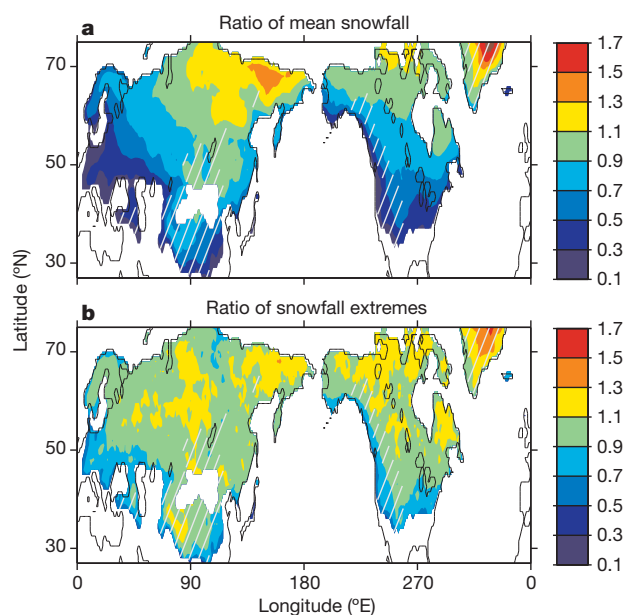

Figure 1 | Ratios of snowfall for the warm climate compared with the control climate. a, b, Multimodel-median ratios (colour scale) of mean snowfall (**a**) and daily snowfall extremes as measured by their 20-year return values (**b**). The 20-year return values were estimated using a fit of the generalized extreme value distribution to the annual-maximum time series. Ratios are only shown for land grid boxes where the multimodel-median of mean snowfall is greater than 5 cm per year in the control climate. White hatching denotes regions with surface elevations above 1,000 m that are not included in Figs 2–4.

[1]Department of Earth, Atmospheric and Planetary Sciences, Massachusetts Institute of Technology, Cambridge, Massachusetts 02139, USA.

response, with substantially smaller fractional changes than for mean snowfall in many regions (Fig. 1b).

Snowfall statistics and their changes are expected to be strongly dependent on the climatological temperature, which varies by month and region. To quantify this dependence, I next analysed the changes in snowfall as a function of the climatological monthly surface air temperature in the control climate. Daily snowfall rates were aggregated in 5 °C bins with centres from –22.5 °C to 12.5 °C according to the climatological monthly surface air temperature in the control climate for each grid box and day. Snowfall extremes were calculated as high percentiles of the daily snowfall rates in each temperature bin, including days with no snowfall. Both mean snowfall and snowfall extremes in the different temperature bins are in good agreement with observational estimates (Extended Data Fig. 3). The response to climate change is first presented for surface elevations below 1,000 m (Extended Data Fig. 4). Fractional decreases are greater for mean snowfall than for snowfall extremes for much of the temperature range considered here (Fig. 2a), which demonstrates the contrasting responses of mean and extreme snowfall even when monthly variations in climatological temperature are controlled for. For the temperature bin centred around −2.5 °C, mean snowfall decreases by 65% in the multimodel median, whereas the 99.99th percentile of snowfall decreases by only 8%. Changes in snowfall extremes transition from positive to negative at control-climate temperatures as high as −9 °C, whereas the corresponding temperature for mean snowfall is −14 °C. Furthermore, the difference in behaviour between mean and extremes is greater the higher the percentile of snowfall considered (Fig. 2a), and this difference is robust across different climate models (Extended Data Fig. 5).

I next present a simple theory that accounts for the main features of the response of snowfall extremes to climate change. The theory does not include the response of mean snowfall, but this has been explained previously in terms of changes in mean precipitation and temperature[3,4]. Surface precipitation type depends on the vertical temperature profile

of the lower troposphere[20], but to first order it may be related to surface air temperature[21,22]. The daily snowfall rate s in the theory is related to the daily precipitation rate p by $s = f(T)p$, where T is the daily surface air temperature, and $f(T)$ is the snowfall fraction (the fraction of precipitation that falls as snow at a given temperature T). The $f(T)$ diagnosed from the simulations shows a sharp decline near freezing (Fig. 3), and this is comparable to what is found in observations (Extended Data Fig. 6). As expected given modest changes in lapse rates (the rates of decrease of temperature with height), $f(T)$ is almost exactly the same in the control and warm climates (Fig. 3).

The daily precipitation rate in the theory is assumed to have a simple dependence on surface air temperature according to $p = e^{\beta T}\hat{p}$, where $\beta = 0.06\,°C^{-1}$ is a representative thermodynamic rate of increase of extratropical precipitation extremes with respect to surface temperature related to changes in saturation-specific humidity[12]. The normalized precipitation variable $\hat{p}$ may be thought of as a dynamic variable closely related to upward motion in the atmosphere; it is assumed to follow a gamma distribution on wet days with scale parameter γ^{-1} and shape parameter k. The fraction of wet days is denoted w. The temperature T is assumed to be normally distributed with mean $\bar{T}$ and standard deviation σ, and $\hat{p}$ and T are taken to be independent.

With these assumptions, asymptotic methods were used to evaluate the integrals over temperature and $\hat{p}$ involved in the calculation of high percentiles of snowfall (Methods). The reciprocal of the temperature dependence of the snowfall rate is denoted $h(T) = e^{-\beta T}f(T)^{-1}$, and the asymptotics show that the behaviour of snowfall extremes is dominated by the temperature T_m at which $h(T)$ reaches a minimum (roughly −2 °C in the simulations and observations). T_m is the optimal temperature for snowfall extremes in the theory, and it arises because of the competition between increasing saturation-specific humidity and decreasing snowfall fraction with increasing temperature. The result is that the qth percentile of snowfall s_q is given by:

$$(\gamma s_q h_m)^{\frac{3}{2}-k}e^{\gamma s_q h_m} = \frac{w}{\sigma\left(1-\frac{q}{100}\right)\Gamma(k)}\sqrt{\frac{h_m}{h_m''}}\,e^{-\frac{(\bar{T}-T_m)^2}{2\sigma^2}} \quad (1)$$

which is valid asymptotically for large s_q values, where Γ is the gamma function, h_m is h evaluated at T_m, and h_m'' is the second derivative of h at T_m. For a change in mean temperature of $\delta\bar{T}$ and assuming negligible changes in all other parameters, the change in snowfall extremes, δs_q, is given by:

$$\delta s_q = -\frac{\delta\bar{T}}{\sigma^2\gamma h_m}\left(\bar{T}+\frac{\delta\bar{T}}{2}-T_m\right) \quad (2)$$

as shown in the Methods.

According to equation (2), δs_q transitions from positive to negative at a mean temperature in the control climate of $T_m - \delta\bar{T}/2$ (roughly equal to −6 °C in the simulations), and it is proportional to $1/(\gamma h_m)$,
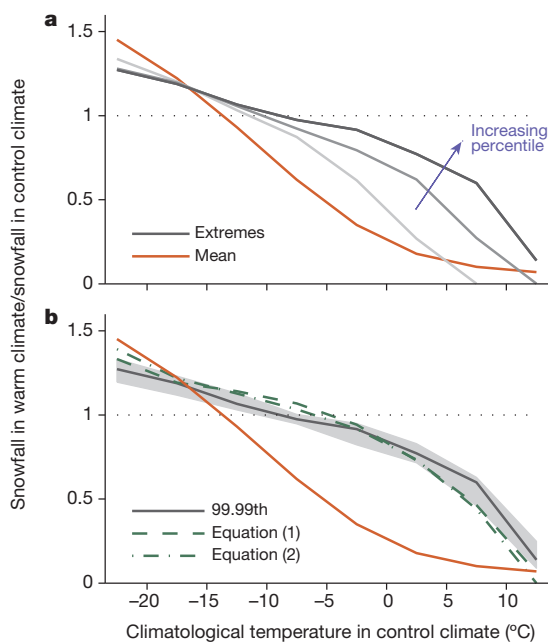

Figure 2 | Ratios of snowfall for the warm climate compared with the control climate as a function of climatological monthly surface air temperature in the control climate. Multimodel-median ratios of mean snowfall (red) in both panels. a, Multimodel-median ratios of the 99th, 99.9th and 99.99th percentiles of daily snowfall in increasing order from light to dark grey. b, Multimodel-median ratio of the 99.99th percentile of daily snowfall (grey line; shading shows the interquartile range), and the same ratio calculated from theory according to equation (1) (green dashed) and equation (2) (green dashed-dotted). Only land grid boxes in the Northern Hemisphere with surface elevation below 1,000 m are included.
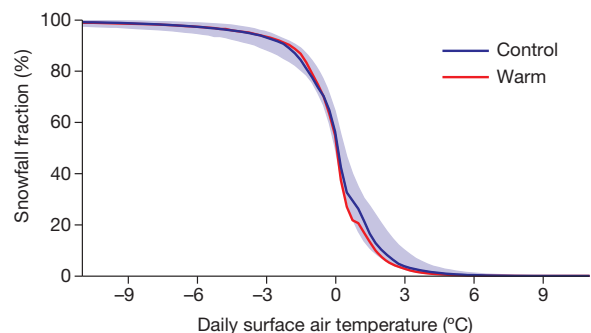

Figure 3 | Daily snowfall fraction as a function of daily surface air temperature. The multimodel-median snowfall fraction is shown for the control climate (blue line; shading shows the interquartile range) and the warm climate (red line). It is calculated in each model and for each climate as the ratio of mean snowfall to mean precipitation in daily temperature bins of width 0.25 °C. Only land grid boxes in the Northern Hemisphere with surface elevation below 1,000 m are included.
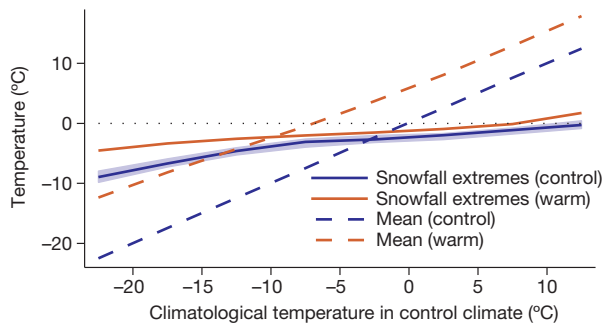
Figure 4 | Multimodel-median surface air temperatures at which snowfall extremes occur as a function of climatological monthly surface air temperature in the control climate. For each control-climate temperature bin, surface air temperatures are averaged over grid boxes and days for which the daily snowfall is at or above its 99.99th percentile in the control climate (blue solid line; shading shows the interquartile range) and warm climate (red solid line). Mean temperatures are also shown (dashed lines). The blue dashed line deviates from a one-to-one relationship only because of sampling variability. Only land grid boxes in the Northern Hemisphere with surface elevation below 1,000 m are included.

which is a characteristic snowfall rate at $T = T_m$. The change δs_q also depends inversely on temperature variability as measured by σ^2, which makes sense given that, for example, temperature variability allows daily temperatures to reach below freezing even if the mean temperature increases to above freezing. Notably, δs_q is independent of the percentile considered, such that the fractional change $\delta s_q/s_q$ is small for sufficiently large s_q. This is the main result from the theory—that the temperature dependencies of precipitation extremes and the rain–snow transition lead to fractional changes in snowfall extremes that are small for sufficiently large snowfall extremes in the control climate. Snowfall extremes respond differently to climate change as compared to precipitation extremes or mean snowfall because snowfall extremes tend to occur at temperatures in a relatively narrow range near the optimal temperature T_m in both the control and warm climates (Fig. 4). As shown schematically in Extended Data Fig. 7, changes in mean temperature do imply changes in the probability of occurrence of temperatures near the optimal temperature for snowfall extremes, but this only results in changes in snowfall extremes that are independent of the percentile considered.

I applied the theory introduced above to the simulations (Methods; Extended Data Fig. 8), and it captures the important features of the response of the snowfall extremes to climate change as a function of climatological monthly temperature (Fig. 2b). (Application of the theory at individual locations is left to future work.) The simulated changes in snowfall extremes asymptote towards the simple theoretical form given by equation (2) as the percentile is increased, and good agreement with the theory is found for the 99.9th and 99.99th percentiles (Extended Data Fig. 9).

Many mountainous regions experience heavy snowfall, but the accuracy of the theory is not as good for regions with surface elevations above 1,000 m (Extended Data Fig. 10), possibly because of variations in the thermodynamic response of orographic precipitation to climate change[23] or the difficulty in simulating orographic snowfall[3]. Nonetheless, the result that fractional decreases in mean snowfall are greater than those in snowfall extremes seems to hold regardless of elevation in the simulations (Fig. 1 and Extended Data Fig. 10).

Changes in snowfall extremes may still have impacts, and large fractional decreases do occur in the simulations for more moderate extremes and for regions and times of year that are warm enough that there is little snowfall in the control climate (Fig. 2). In addition, changes in the probability of exceeding a fixed high threshold of snowfall (that is, changes in the frequency rather than the intensity of snowfall extremes) may still be substantial because of the exponential tail of precipitation distributions (Extended Data Fig. 7b). Changes in the frequency of snowfall extremes cannot be directly compared with changes in mean snowfall,

but they may be important for impacts that involve a fixed threshold of snowfall. Previous work suggests that the regional climate-change signal of mean snowfall will only emerge after that of temperature, despite large reductions in mean snowfall in many regions[4,24]. The relatively small fractional changes in snowfall extremes found here suggest that snowfall extremes may not be an early indicator of climate change in many regions; if so, this has corresponding implications for the detection and public perception of climate change.

1. Räisänen, J. Warmer climate: less or more snow? *Clim. Dyn.* **30,** 307–319 (2008).
2. Brown, R. D. & Mote, P. W. The response of northern hemisphere snow cover to a changing climate. *J. Clim.* **22,** 2124–2145 (2009).
3. Kapnick, S. B. & Delworth, T. L. Controls of global snow under a changed climate. *J. Clim.* **26,** 5537–5562 (2013).
4. Krasting, J. P., Broccoli, A. J., Dixon, K. & Lanzante, J. Future changes in northern hemisphere snowfall. *J. Clim.* **26,** 7813–7828 (2013).
5. Rooney, J. F. Jr. The urban snow hazard in the United States: an appraisal of disruption. *Geogr. Rev.* **57,** 538–559 (1967).
6. Kocin, P. J. & Uccellini, L. W. *Northeast Snowstorms* Ch. 1 (American Meteorological Society, 2004).
7. Changnon, S. A. & Changnon, D. A spatial and temporal analysis of damaging snowstorms in the United States. *Nat. Hazards* **37,** 373–389 (2006).
8. Min, S. K., Zhang, X., Zwiers, F. W. & Hegerl, G. C. Human contribution to more-intense precipitation extremes. *Nature* **470,** 378–381 (2011).
9. Westra, S., Alexander, L. V. & Zwiers, F. W. Global increasing trends in annual maximum daily precipitation. *J. Clim.* **26,** 3904–3918 (2013).
10. Kharin, V. V., Zwiers, F. W., Zhang, X. & Wehner, M. Changes in temperature and precipitation extremes in the CMIP5 ensemble. *Clim. Change* **119,** 345–357 (2013).
11. Trenberth, K. E. Conceptual framework for changes of extremes of the hydrological cycle with climate change. *Clim. Change* **42,** 327–339 (1999).
12. O'Gorman, P. A. & Schneider, T. The physical basis for increases in precipitation extremes in simulations of 21st-century climate change. *Proc. Natl Acad. Sci. USA* **106,** 14773–14777 (2009).
13. O'Gorman, P. A. & Schneider, T. Scaling of precipitation extremes over a wide range of climates simulated with an idealized GCM. *J. Clim.* **22,** 5676–5685 (2009).
14. Kunkel, K. E. *et al.* Monitoring and understanding trends in extreme storms: state of knowledge. *Bull. Am. Meteorol. Soc.* **94,** 499–514 (2013).
15. Zhang, X., Hogg, W. D. & Mekis, É. Spatial and temporal characteristics of heavy precipitation events over Canada. *J. Clim.* **14,** 1923–1936 (2001).
16. Kunkel, K. E. *et al.* Trends in twentieth-century U.S. extreme snowfall seasons. *J. Clim.* **22,** 6204–6216 (2009).
17. Diffenbaugh, N. S., Scherer, M. & Ashfaq, M. Response of snow-dependent hydrologic extremes to continued global warming. *Nature Clim. Change* **3,** 379–384 (2013).
18. Changnon, S. A., Changnon, D. & Karl, T. R. Temporal and spatial characteristics of snowstorms in the contiguous United States. *J. Appl. Meteorol. Climatol.* **45,** 1141–1155 (2006).
19. Kodra, E., Steinhaeuser, K. & Ganguly, A. R. Persisting cold extremes under 21st-century warming scenarios. *Geophys. Res. Lett.* **38,** L08705 (2011).
20. Bourgouin, P. A method to determine precipitation types. *Weath. Forecast.* **15,** 583–592 (2000).
21. Dai, A. Temperature and pressure dependence of the rain-snow phase transition over land and ocean. *Geophys. Res. Lett.* **35,** L12802 (2008).
22. Feiccabrino, J., Gustafsson, D. & Lundberg, A. Surface-based precipitation phase determination methods in hydrological models. *Hydrol. Res.* **44,** 44–57 (2013).
23. Siler, N. & Roe, G. How will orographic precipitation respond to surface warming? An idealized thermodynamic perspective. *Geophys. Res. Lett.* **41,** 2606–2613 (2014).
24. Pierce, D. W. & Cayan, D. R. The uneven response of different snow measures to human-induced climate warming. *J. Clim.* **26,** 4148–4167 (2013).

METHODS

Simulations. The 20 climate models used were BNU-ESM, CanESM2, CMCC-CESM, CMCC-CM, CMCC-CMS, CSIRO-Mk3-6-0, GFDL-CM3, GFDL-ESM2G, GFDL-ESM2M, HadGEM2-CC, HadGEM2-ES, IPSL-CM5A-LR, IPSL-CM5A-MR, IPSL-CM5B-LR, MIROC5, MIROC-ESM-CHEM, MIROC-ESM, MPI-ESM-LR, MPI-ESM-MR and MRI-CGCM3. The time period used for HadGEM2-ES for RCP 8.5 was 2081–2099 rather than 2081–2100 because only those years were available in the archive. The first ensemble member was used in all cases.

For Extended Data Fig. 5, a subset of ten models was chosen in which only one model is included from each modelling centre: 1. BNU-ESM, 2. CanESM2, 3. CMCC-CM, 4. CSIRO-Mk3-6-0, 5. GFDL-CM3, 6. HadGEM2-CC, 7. IPSL-CM5A-MR, 8. MIROC5, 9. MPI-ESM-MR, and 10. MRI-CGCM3. These models were selected as either the most recent or the highest resolution in each case.

Calculation of daily snowfall extremes. I calculated snowfall extremes in two ways. In the first method, 20-year return values were calculated from annual maxima using the generalized extreme value (GEV) distribution to allow for relatively-long return periods at each grid box. In the second method, daily snowfall rates were aggregated in bins according to the climatological monthly surface air temperature in the control climate, and high percentiles of snowfall were estimated in each bin; this takes into account the sensitive dependence of snowfall on climatological monthly temperature and allows for a straightforward comparison with theory.

In the first method (Fig. 1 and Extended Data Figs 1 and 2), 20-year return values of daily snowfall were calculated for each model or observational data set, grid box and climate. The 20-year return values were calculated from time series of annual maxima by fitting the GEV distribution using probability-weighted moments[25]. Probability-weighted moments were used rather than maximum-likelihood estimation because of the relatively short samples, and this approach has been previously used for precipitation extremes[26] and to analyse CMIP5 output[10]. The goodness of fit was assessed using a Monte Carlo version of the Kolmogorov–Smirnov test[26]. (A Monte Carlo version of the test was needed because the null hypothesis involves parameters estimated from the time series.) Land grid boxes in the Northern Hemisphere with mean snowfall of greater than 5 cm per year in liquid-water equivalent were considered. The fraction of these grid boxes at which the test was passed at the 10% significance level was found to be close to 10%; the goodness of fit declines if grid boxes with mean snowfall lower than 5 cm per year are included in the analysis. As an additional check, return values were directly estimated as empirical quantiles of the annual maxima time series, and similar results to the GEV estimates were found for a range of quantiles. For the results that are presented as maps, the snowfall statistics were interpolated to a common grid before calculation of multimodel medians. The conclusions are similar if the snowfall extremes are instead measured by the 10-year or 50-year return values (not shown), although the 50-year return values must be viewed with caution given that the underlying time series span roughly 20 years.

In the second method (see Fig. 2), snowfall statistics were analysed as a function of climatological monthly surface air temperature in the control climate. Snowfall extremes were calculated as empirical quantiles of the daily snowfall rates in each temperature bin (without using the GEV distribution in this case). All days, including days with zero snowfall, were included in the analysis. The sample size of snowfall rates in a given temperature bin is of the order of 10^6, and the 99th, 99.9th and 99.99th percentiles were calculated.

Comparison of simulations with observations. The mean snowfall and snowfall extremes in the simulations are compared with observational estimates in Extended Data Figs 1, 2 and 3. Previous global-scale modelling studies have compared simulated snowfall rates with snowfall rates from reanalysis[3] or monthly snowfall rates derived empirically from monthly precipitation rates and monthly surface temperatures[4]. Because observational estimates of daily snowfall are needed and because snowfall from reanalysis may be unreliable[3], snowfall rates were estimated here on the basis of observed daily precipitation rates and surface air temperatures and the observed dependence of snowfall fraction on temperature. (Mean snowfall from CloudSat is also discussed below.) The precipitation rates are over the period 1997–2012 and were taken from the one-degree daily merged product V1.2 of the Global Precipitation Climatology Project (GPCP 1DD), which includes inputs from infrared, passive microwave, and gauge measurements[27]. The precipitation rates were first interpolated to a coarser grid with a grid spacing of 2° that is comparable to that of the climate models. Conservative interpolation was used to be consistent with the treatment of precipitation as a flux[28]. The daily surface air temperatures were taken from the NCEP-DOE reanalysis 2 (NCEP2)[29]. The dependence of snowfall fraction on temperature was taken from a study of precipitation at Swedish meteorological stations[22] (Extended Data Fig. 6) and is given by $\exp[-0.0000858(T + 7.5)^{4.12}]$ when the surface air temperature T (in degrees Celsius) is between $-4\,°C$ and $7\,°C$. All snow was assumed to occur at temperatures below $-4\,°C$ and all rain at temperatures above $7\,°C$. The snowfall observations are for three-hourly rather than daily accumulations, but this is not expected to affect the results presented particularly

strongly. For example, the good agreement between models and observations shown in Extended Data Fig. 3 is retained if a simple threshold of $1\,°C$ is used to determine precipitation type for the GPCP-based observations (that is, assuming all snow below $1\,°C$ and all rain above it).

In addition, mean snowfall data from CloudSat[30] were used to provide a second and independent comparison with observations (Extended Data Figs 1 and 3). The CloudSat product used (2C-SNOW-PROFILE Release 4) includes vertical profiles of snowfall rate and surface snowfall rate based on reflectivity profiles from the CloudSat Cloud Profiling Radar[31]. The data were available for the period mid-July 2006 to mid-April 2011, which is sufficient to evaluate the mean snowfall rates but is too short to allow for estimation of snowfall extremes.

The overall magnitude and pattern of mean and extreme snowfall are captured by the simulations but with some regional discrepancies (Extended Data Figs 1 and 2). When interpreting the model and observational maps of snowfall, it is important to take into account the area-averaging to a coarse grid and the use of liquid-water equivalent rather than snowfall depth. Snowfall biases in the models may partly relate to temperature biases[4] and inadequate spatial resolution in regions with high topography[3]. There are also regional differences in mean snowfall between the two observational estimates (Extended Data Fig. 1), although these differences may relate in part to the different time periods used.

The agreement between the models and the observations is very good when mean and extreme snowfall are analysed as a function of climatological temperature in the control climate (Extended Data Fig. 3). That agreement is better in this case is probably because mean temperature biases are less important when snowfall is analysed as a function of climatological temperature and because variability, circulation biases and random errors are averaged over space and time in each temperature bin. In addition, there is good agreement between the two observational estimates for mean snowfall, except in the lowest temperature bin (Extended Data Fig. 3, bottom panel).

A comparison of the observed snowfall fraction with the snowfall fraction in the simulations (including all surface elevations as in the observations) suggests that the snowfall fraction in the multimodel median is accurate for temperatures below $0\,°C$ but declines to zero slightly too quickly for temperatures above $0\,°C$ (Extended Data Fig. 6). The discrepancy above $0\,°C$ could also result in part from the inexact nature of the comparison between station data and model grid boxes and from the difficulty of apportioning mixed snow and rain in observations. This discrepancy does not affect the optimal temperature T_m in the theory of snowfall extremes because $T_m < 0\,°C$. Note that the rain–snow transition does not occur precisely at a surface temperature of $0\,°C$ because frozen precipitation does not immediately melt as it falls past the melting level and because of temperature variability within the accumulation period used.

Derivation of theory for snowfall extremes. The following assumptions are made in the derivation, as discussed in the main text. The daily snowfall rate s is related to the daily precipitation rate p and daily surface air temperature T according to $s = f(T)p$, where $f(T)$ is the fraction of precipitation that falls as snow at a given temperature T. The daily surface air temperature T is assumed to be normally distributed with mean $\bar{T}$ and standard deviation σ. The precipitation rate p has a simple dependence on T according to $p = e^{\beta T}\hat{p}$. This exponential dependence on temperature is motivated by the thermodynamic scaling of precipitation extremes under climate change[12] and the observed covariability of daily precipitation extremes with surface temperature[32]. The normalized precipitation rate $\hat{p}$ is assumed to follow a gamma distribution on wet days[33], such that its probability density function P is given by:

$$P(\hat{p}) = (1-w)\delta(\hat{p}) + \frac{w\gamma^k}{\Gamma(k)}\hat{p}^{k-1}e^{-\gamma\hat{p}}$$

where δ is the delta function, Γ is the gamma function, w is the fraction of wet days, $1/\gamma$ is the scale parameter and k is the shape parameter. (When applying the theory to the simulations, wet days are defined as days with precipitation greater than 0.1 mm per day rather than precipitation greater than zero, as described here.) The temperature T and the normalized precipitation rate $\hat{p}$ are assumed to be independent.

With these assumptions, the qth percentile of snowfall s_q is exceeded if the following inequality is satisfied:

$$\hat{p}\,e^{\beta T}f(T) > s_q$$

which requires that $\hat{p} > h(T)s_q$, where $h(T) = e^{-\beta T}f(T)^{-1}$. Assuming s_q is non-zero, the probability that s_q is exceeded may be written as:

$$1 - \frac{q}{100} = \int_{-\infty}^{\infty}\mathrm{d}T\int_{h(T)s_q}^{\infty}\mathrm{d}\hat{p}\,\frac{w\gamma^k}{\Gamma(k)}\hat{p}^{k-1}e^{-\gamma\hat{p}}\frac{1}{\sqrt{2\pi}\sigma}e^{-\frac{(T-\bar{T})^2}{2\sigma^2}} \qquad (3)$$

Asymptotic methods are next used to evaluate the double integral in equation (3) in the extreme snowfall limit of large s_q. The integral in $\hat{p}$ is first evaluated using

a standard asymptotic expression for the incomplete gamma function[34]:

$$\int_z^\infty dt\, t^{k-1} e^{-t} = z^{k-1} e^{-z} \left[1 + O(z^{-1}) \right] \qquad (4)$$

in the limit of large and positive z. Making the identifications

$$t = \gamma \hat{p}$$

$$z = \gamma h s_q$$

in equation (4) gives:

$$\int_{\gamma h s_q}^\infty d(\gamma \hat{p})(\gamma \hat{p})^{k-1} e^{-\gamma \hat{p}} = (\gamma h s_q)^{k-1} e^{-\gamma h s_q} \qquad (5)$$

which is valid asymptotically for large s_q. (The tilde symbol to denote 'is asymptotic to' is not used here, to avoid confusion with its common use to denote scaling behaviour.) Note that $\gamma > 0$ and $h(T) > 0$. Substituting equation (5) into equation (3) gives:

$$1 - \frac{q}{100} = \frac{(\gamma s_q)^{k-1} w}{\Gamma(k)\sqrt{2\pi}\sigma} \int_{-\infty}^\infty dT\, h(T)^{k-1} e^{-\gamma h(T) s_q - \frac{(T-\bar{T})^2}{2\sigma^2}} \qquad (6)$$

For large s_q, the integral in temperature is dominated by the contribution close to $T = T_m$ at which $h(T)$ reaches a minimum, which corresponds physically to snowfall extremes occurring near the optimal temperature T_m (found to be roughly $-2\,°C$). The integral may be evaluated asymptotically using Laplace's method[35], and the general result used here is:

$$\int_{-\infty}^\infty dt\, g(t) e^{x\phi(t)} = \sqrt{\frac{2\pi}{-x\phi''(c)}}\, g(c) e^{x\phi(c)} \left[1 + O(x^{-1}) \right] \qquad (7)$$

as $x \to \infty$, where the function ϕ reaches a maximum at $t = c$, and the first and second derivatives of ϕ are denoted ϕ' and ϕ'', respectively. Here

$$x = \gamma s_q$$

$$t = T$$

$$c = T_m$$

$$g(t) = h(T)^{k-1} e^{-\frac{(T-\bar{T})^2}{2\sigma^2}}$$

$$\phi(t) = -h(T)$$

and ϕ reaches a maximum when h reaches a minimum. These substitutions are used in equation (7) to give:

$$\int_{-\infty}^\infty dT\, h(T)^{k-1} e^{-\gamma h(T) s_q - \frac{(T-\bar{T})^2}{2\sigma^2}} = \sqrt{\frac{2\pi}{\gamma s_q h_m''}}\, h_m^{k-1} e^{-\gamma s_q h_m - \frac{(T_m-\bar{T})^2}{2\sigma^2}}$$

which is valid asymptotically for large s_q, and where the subscript 'm' refers to a quantity evaluated at $T = T_m$. Substituting this into equation (6) yields equation (1) in the main text. Equation (1) can always be solved for s_q if $k < \frac{3}{2}$, as is generally the case in the simulations (Extended Data Fig. 8).

Derivation of simple expression for changes in snowfall extremes. The change in s_q may be calculated by evaluating s_q from equation (1) in each climate and taking the difference. Alternatively, a simple expression is derived here for the change in s_q, assuming that all parameters other than the mean temperature $\bar{T}$ remain constant. The changes in s_q and $\bar{T}$ between the control and warm climate are denoted δs_q and $\delta \bar{T}$, respectively. Taking the ratio of the left-hand side of equation (1) in the warm and control climates and equating it to the same ratio for the right-hand side yields:

$$\frac{(s_q + \delta s_q)^{\frac{3}{2}-k}}{s_q^{\frac{3}{2}-k}} e^{\gamma h_m \delta s_q} = e^{-\frac{1}{2\sigma^2}\left[(\bar{T}+\delta\bar{T}-T_m)^2 - (\bar{T}-T_m)^2\right]}$$

Taking the logarithm and rearranging terms gives:

$$\frac{\delta s_q}{s_q} = -\frac{\delta \bar{T}}{\sigma^2 \gamma h_m s_q}\left(\bar{T} + \frac{\delta \bar{T}}{2} - T_m\right) + \frac{k-\frac{3}{2}}{\gamma h_m s_q}\log\left(1 + \frac{\delta s_q}{s_q}\right) \qquad (8)$$

Since the limit of $s_q \to \infty$ is being taken, equation (8) implies that $\delta s_q/s_q \to 0$. The alternative limits $\delta s_q \to -s_q$ or $\delta s_q/s_q \to \infty$ in which the logarithm on the right-hand

side of equation (8) becomes large in magnitude are inconsistent with equation (8) because $k < \frac{3}{2}$. Because $\delta s_q/s_q \to 0$, the second term on the right-hand side of equation (8) may then be neglected, and equation (2) in the main text is obtained.

According to equation (2), the change in snowfall extremes is independent of q, w, k and h_m''. If it is found that $\delta s_q < -s_q$ when applying equation (2), then the starting point given by equation (3) is invalid because it assumes $s_q > 0$, and we must instead set $\delta s_q = -s_q$. Note that unlike equation (2), equation (1) has the accidental advantage of always implying non-negative snowfall rates even when the assumptions made in its derivation are not accurate.

Application of the theory to the simulations. The snowfall fraction $f(T)$ is needed to calculate $h(T)$ and the optimal temperature T_m. It was calculated for each model and climate by binning the daily precipitation and snowfall rates in surface air temperature bins of $0.25\,°C$ over land in the Northern Hemisphere and below or above $1{,}000\,m$ elevation as required (Fig. 3). Because the second derivative of $h(T)$ was needed, the diagnosed $f(T)$ was smoothed using a Gaussian filter with standard deviation $0.5\,°C$ before calculation of $h(T)$. The multimodel medians of T_m and $f(T_m)$ are $-2.3\,°C$ and 0.89, respectively, in both the control climate and warm climate, for the default case of surface elevations below $1{,}000\,m$. The functional fit to the snowfall fraction from observations[22] discussed earlier yields similar values of $T_m = -2.3\,°C$ and $f(T_m) = 0.93$.

The parameter describing the thermodynamic dependence of precipitation extremes was set to $\beta = 0.06\,°C^{-1}$, following previous work[12]. The other parameters in the theory were evaluated for each control-climate temperature bin using the temperatures and precipitation rates aggregated within the bin. Wet days were defined to occur when precipitation is at or above $0.1\,mm$ per day, and the gamma distribution was fitted to wet-day values of $\hat{p}$ using the method of moments to estimate γ and k (Extended Data Fig. 8).

The theory tends to underestimate the absolute magnitudes of the snowfall extremes for the 99.99th percentile (Extended Data Fig. 4), although the fractional changes between climates are still accurate (Fig. 2b). The underestimate of the absolute magnitudes of the 99.99th percentiles results primarily from inaccuracies in the fit of the gamma distribution to the distribution of $\hat{p}$. The method of moments was used to fit the gamma distribution because it was found to give a better fit than maximum-likelihood estimation for the moderate and extreme parts of the $\hat{p}$ distribution. One potential change to the theory would be to fit alternative distributions[36] for $\hat{p}$, although not all distributions allow for asymptotic evaluation of the integrals needed to calculate the snowfall extremes and thus would not lead to a simple result. In the section 'Alternative form of theory using Weibull distribution' below, I show that the theory may still be evaluated asymptotically when the Weibull distribution is used instead of the gamma distribution. The conclusions are similar, with the primary difference being that greater deviations from an exponential tail are possible than with the gamma distribution, and these deviations can lead to a weak dependence of the changes in snowfall extremes on the percentile considered.

The theory also assumes that $\hat{p}$ (a proxy for upward motion) and temperature are independent, but upward motion and precipitation are generally less likely to occur on anomalously cold days[37], and the accuracy of the theory could be improved by accounting for this relationship. This refinement to the theory is not attempted here because of the additional complexity and assumptions needed and because the current form of the theory adequately captures the main features of the response of daily snowfall extremes to climate change.

Alternative form of theory using Weibull distribution. The theory is also tractable if the normalized precipitation rate $\hat{p}$ is assumed to follow a Weibull distribution on wet days instead of a gamma distribution. The probability density function P for $\hat{p}$ is then given by:

$$P(\hat{p}) = (1-w)\delta(\hat{p}) + wl\alpha(\alpha\hat{p})^{l-1} e^{-(\alpha\hat{p})^l}$$

where δ is the delta function, w is the fraction of wet days, $1/\alpha$ is the scale parameter, and l is the shape parameter. In calculating the qth percentile of snowfall, the integral in $\hat{p}$ is exact, and the integral in T is performed using Laplace's method as before. The result is:

$$(\alpha s_q h_m)^{l/2} e^{(\alpha s_q h_m)^l} = \frac{w}{\sigma\left(1 - \frac{q}{100}\right)} \sqrt{\frac{h_m^l}{(h^l)_m''}}\, e^{-\frac{(\bar{T}-T_m)^2}{2\sigma^2}}$$

The simple expression for the change in s_q, corresponding to equation (2) when the gamma distribution is used, is given by:

$$\delta s_q = -\frac{\delta\bar{T}}{\sigma^2 l(\alpha h_m)^l (s_q)^{l-1}}\left(\bar{T} + \frac{\delta\bar{T}}{2} - T_m\right) \qquad (9)$$

The parameters in the Weibull distribution were estimated using maximum-likelihood estimation, and the results for the changes in snowfall extremes were

found to be similar to the results from the theory using the gamma distribution (not shown). According to equation (9), the change in snowfall extremes δs_q depends on $(s_q)^{l-1}$ and therefore is no longer completely independent of the percentile to the extent that l differs from 1. However, this dependence was found to be weak, and typical values of l in the simulations are in the range 0.7–1.1. Importantly, it is still the case that the fractional change $\delta s_q / s_q$ is small for sufficiently large s_q because $l > 0$.

Role of circulation changes and robustness of results. In the theory, γ and k are the parameters that are most strongly tied to dynamics and updraft strength. These parameters do change to some extent as the climate warms (Extended Data Fig. 8), but they do not change sufficiently to alter the large contrast between the changes in mean and extreme snowfall, and similar results are found whether snowfall extremes are estimated from the full theory given by equation (1) or if the simple estimate given by equation (2) is used that assumes parameters such as γ and k are fixed (Fig. 2b). The ratios from equation (2) are calculated as $1 + \delta s_q / s_q$, where all parameters other than the temperature change are evaluated from the control climate.

Much of the uncertainty in changes in upward velocities in climate-model simulations is thought to relate to parameterized moist convection[38,39], which is more important for warm-season or tropical precipitation, even if convection may enhance snowfall locally in a given storm. Consistent with this interpretation, extratropical precipitation extremes are generally found to respond to climate change in a robust manner, unlike tropical precipitation extremes[12,39]. Inaccuracy in simulating Arctic sea-ice loss could affect the warming pattern and circulation, but this would not be expected to alter the contrast between the responses of mean and extreme daily snowfall substantially, and similar results are found here for the subset of models that have previously been identified[40] as performing well when simulating Arctic sea ice (not shown).

Extended Data Fig. 5 illustrates the robustness of the greater declines in mean snowfall as compared to snowfall extremes. To increase the extent to which the models are independent, a subset of ten models with only one model from each climate centre was analysed (see the 'Simulations' section for the list of models). Extended Data Fig. 5a shows that there are widespread regions in which snowfall extremes (as measured by the 20-year return period) fractionally decrease by less than mean snowfall (or increase) in all ten of the models considered. Extended Data Fig. 5b shows that for each of the models separately the fractional decrease in snowfall extremes is robustly less than that in mean snowfall for the $-2.5\,^\circ\mathrm{C}$ control-climate temperature bin.

Heuristic argument for changes in snowfall extremes. The simple estimate given by equation (2) may also be obtained using a heuristic argument based on the property that snowfall extremes tend to occur at temperatures close to T_m in both the control and warm climates (Fig. 4). Consider the case, illustrated in Extended Data Fig. 7, in which the mean temperature is above T_m in the control climate. The joint probability density function (PDF) of temperature T and normalized precipitation $\hat{p}$ is the product of a Gaussian distribution in temperature and a gamma distribution in $\hat{p}$. An increase in mean temperature reduces the joint PDF in the preferred temperature range for extreme snowfall near T_m (Extended Data Fig. 7a), with the result that high percentiles of $\hat{p}$ and snowfall must also decrease (Extended Data Fig. 7b). The integral of the joint PDF over $\hat{p} > s_q h_\mathrm{m}$ at $T = T_\mathrm{m}$ must remain approximately the same in each climate because the percentile considered is unchanged. At $T = T_\mathrm{m}$, the joint PDF has an exponential dependence on $-(T_\mathrm{m} - \bar{T})^2 / (2\sigma^2) - \gamma \hat{p}$, and considering only the exponential part for simplicity, we find that $-\delta\left[(T_\mathrm{m} - \bar{T})^2 / (2\sigma^2)\right] - \gamma \delta s_q h_\mathrm{m} = 0$. In the limit of a small change in mean temperature, we find that $\delta s_q = \delta \bar{T} (T_\mathrm{m} - \bar{T}) / (\sigma^2 \gamma h_\mathrm{m})$, which is consistent with equation (2). So the increase in mean temperature reduces the snowfall extremes in this case, but by an amount that is independent of the percentile considered, such that the change is a small fraction of the snowfall extreme in the control climate for sufficiently high percentiles.

Snowfall depth versus liquid-water equivalent. Snowfall is expressed in liquid-water equivalent in the simulations, but snowfall depth is often measured in observations[41]. Snowfall depth depends on snow density in addition to the liquid-water equivalent, and snow density depends on temperature as well as other factors. The theory of snowfall extremes described above may be easily modified to apply to snowfall depth by assuming a functional dependence of snow density on temperature and including this dependence in the expression relating snowfall and precipitation rates. The snowfall extremes measured in snowfall depth would then be associated with a lower optimal temperature T_m than those measured in liquid-water equivalent (for example, using equations (1) and (2) of ref. 42 for the density of snow together with the observed snowfall fraction curve[22] yields $T_\mathrm{m} = -4.3\,^\circ\mathrm{C}$), but the basic features of the contrast between the responses of mean snowfall and snowfall extremes remain the same.

25. Hosking, J. R. M., Wallis, J. R. & Wood, E. F. Estimation of the generalized extreme-value distribution by the method of probability-weighted moments. *Technometrics* **27,** 251–261 (1985).
26. Kharin, V. V. & Zwiers, F. W. Changes in the extremes in an ensemble of transient climate simulations with a coupled atmosphere-ocean GCM. *J. Clim.* **13,** 3760–3788 (2000).
27. Huffman, G. J. et al. Global precipitation at one-degree daily resolution from multisatellite observations. *J. Hydrometeorol.* **2,** 36–50 (2001).
28. Chen, C. T. & Knutson, T. On the verification and comparison of extreme rainfall indices from climate models. *J. Clim.* **21,** 1605–1621 (2008).
29. Kanamitsu, M. et al. NCEP–DOE AMIP-II reanalysis (R-2). *Bull. Am. Meteorol. Soc.* **83,** 1631–1643 (2002).
30. Stephens, G. L. et al. CloudSat mission: performance and early science after the first year of operation. *J. Geophys. Res.* **113,** D00A18 (2008).
31. Wood, N. Level 2c snow profile process description and interface control document, version 0. http://www.cloudsat.cira.colostate.edu/dataICDlist.php?go=list&path=/2C-SNOW-PROFILE (2013).
32. Lenderink, G. & van Meijgaard, E. Increase in hourly precipitation extremes beyond expectations from temperature changes. *Nature Geosci.* **1,** 511–514 (2008).
33. Groisman, P. Y. et al. Changes in the probability of heavy precipitation: Important indicators of climatic change. *Clim. Change* **42,** 243–283 (1999).
34. Abramowitz, M. & Stegun, I. A. *Handbook of Mathematical Functions: With Formulas, Graphs, and Mathematical Tables* Vol. 55, section 6.5.32 (Dover, 1964).
35. Bender, C. M. & Orszag, S. A. *Advanced Mathematical Methods for Scientists and Engineers I: Asymptotic Methods and Perturbation Theory* Vol. 1, Ch. 6 (Springer, 1999).
36. Furrer, E. M. & Katz, R. W. Improving the simulation of extreme precipitation events by stochastic weather generators. *Water Resourc. Res.* **44,** W12439 (2008).
37. de Vries, H., Haarsma, R. J. & Hazeleger, W. On the future reduction of snowfall in western and central Europe. *Clim. Dyn.* **41,** 2319–2330 (2013).
38. Wilcox, E. M. & Donner, L. J. The frequency of extreme rain events in satellite rain-rate estimates and an atmospheric general circulation model. *J. Clim.* **20,** 53–69 (2007).
39. O'Gorman, P. A. Sensitivity of tropical precipitation extremes to climate change. *Nature Geosci.* **5,** 697–700 (2012).
40. Massonnet, F. et al. Constraining projections of summer Arctic sea ice. *Cryosphere* **6,** 1383–1394 (2012).
41. Paulhus, J. L. H. Record snowfall of April 14–15, 1921, at Silver Lake, Colorado. *Mon. Weath. Rev.* **81,** 38–40 (1953).
42. Brown, R. D., Brasnett, B. & Robinson, D. Gridded North American monthly snow depth and snow water equivalent for GCM evaluation. *Atmosphere–Ocean* **41,** 1–14 (2003).
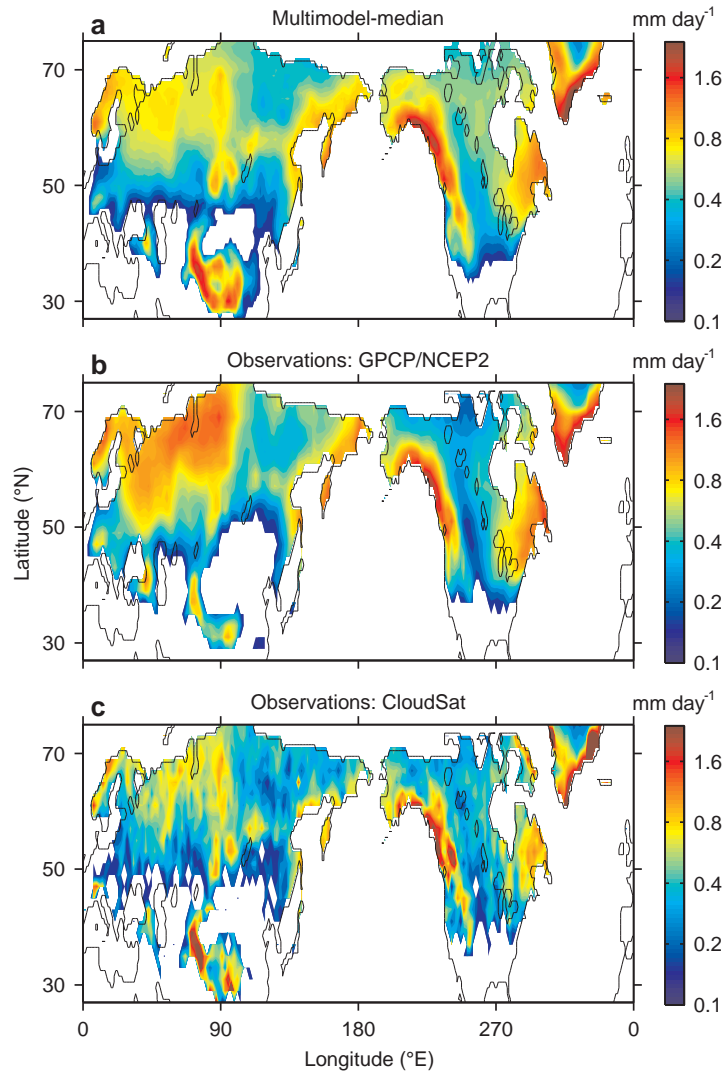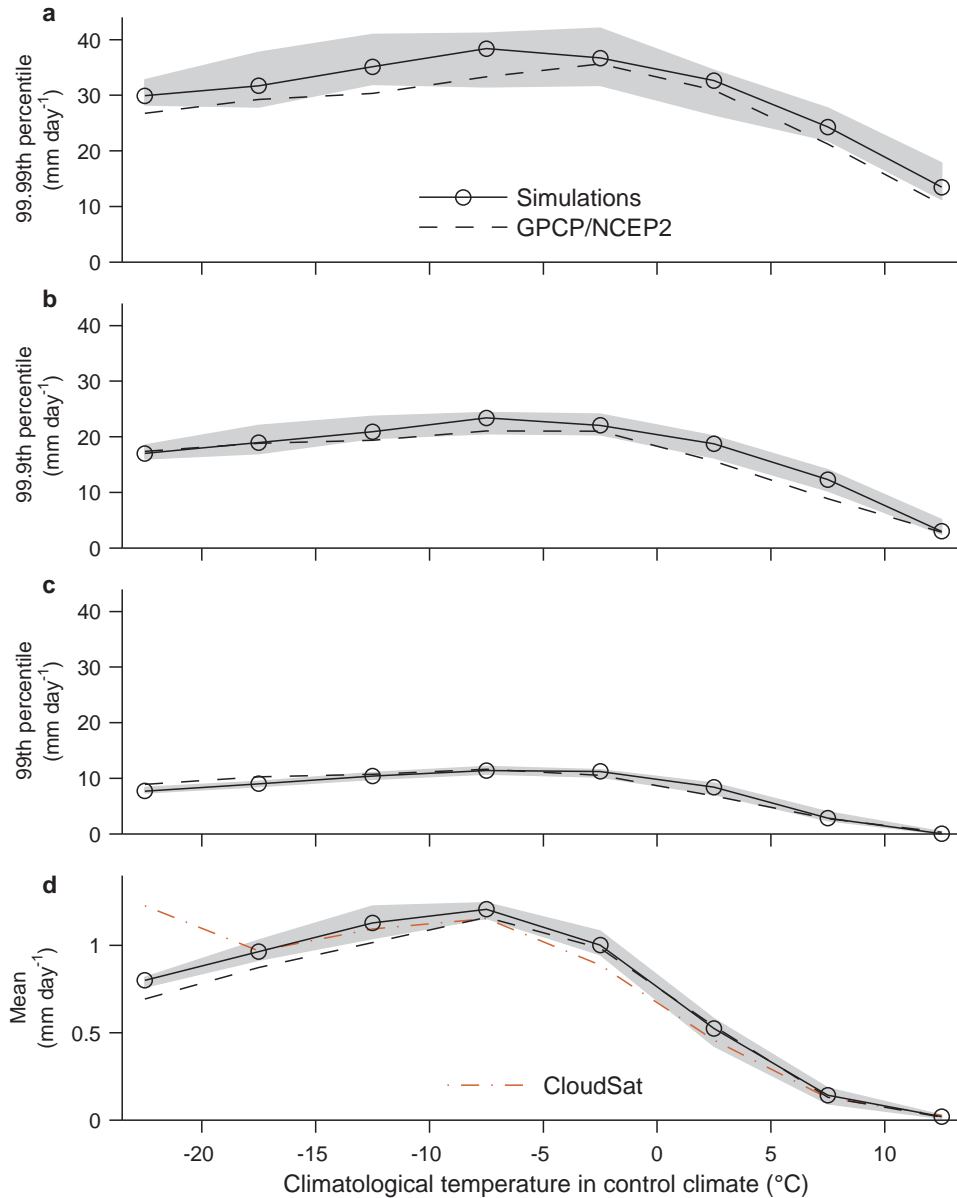
Extended Data Figure 1 | Mean snowfall in simulations and observations. **a**, The control climate in the multimodel median. **b**, **c**, Observational estimates from GPCP/NCEP2 (**b**) and CloudSat (**c**). In each case, results are only shown where mean snowfall exceeds 5 cm per year.
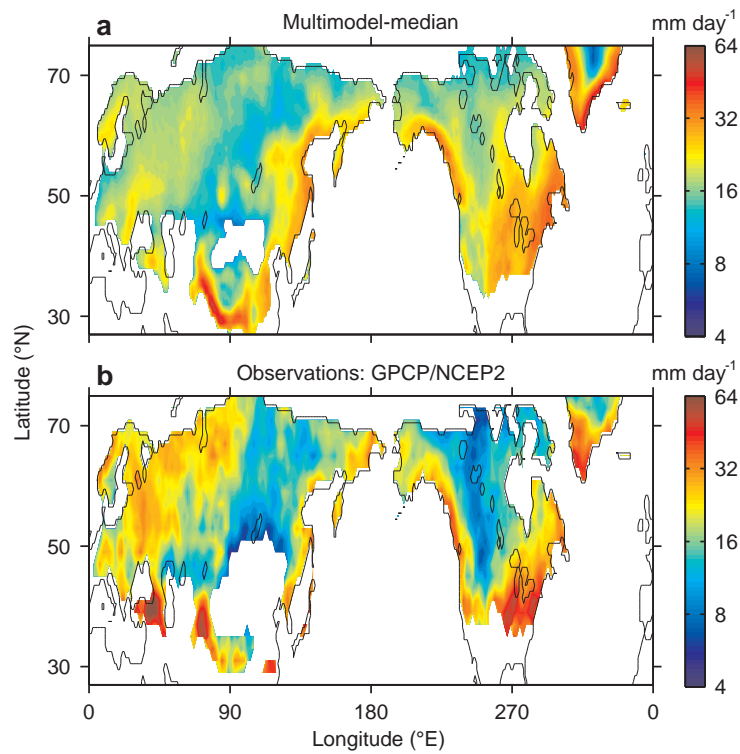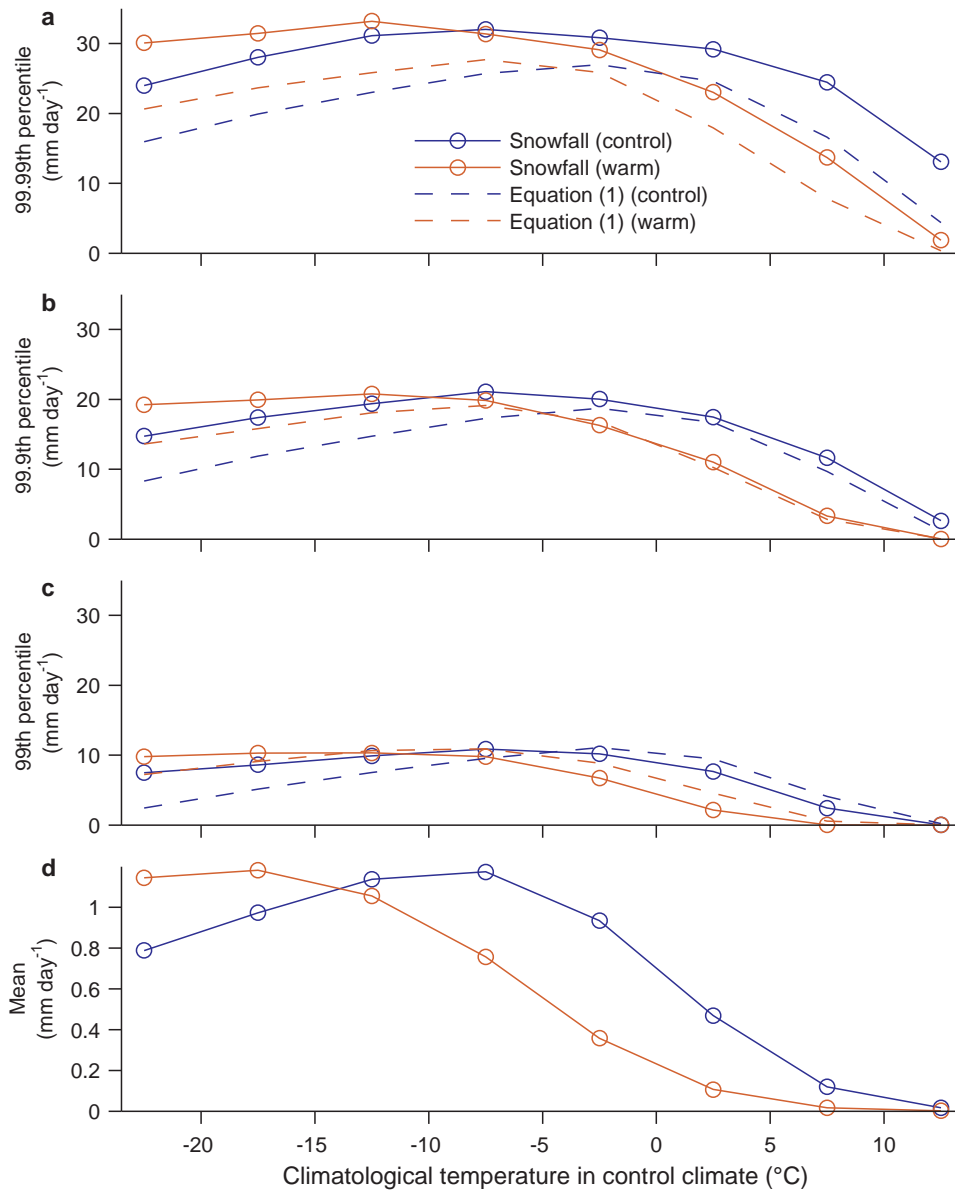
Extended Data Figure 2 | Daily snowfall extremes in simulations and observations. **a**, The control climate in the multimodel median. **b**, Observational estimate from GPCP/NCEP2. The snowfall extremes shown are the 20-year return values estimated using a fit of the generalized extreme value distribution to the annual-maximum time series. In each case, results are only shown where mean snowfall exceeds 5 cm per year.
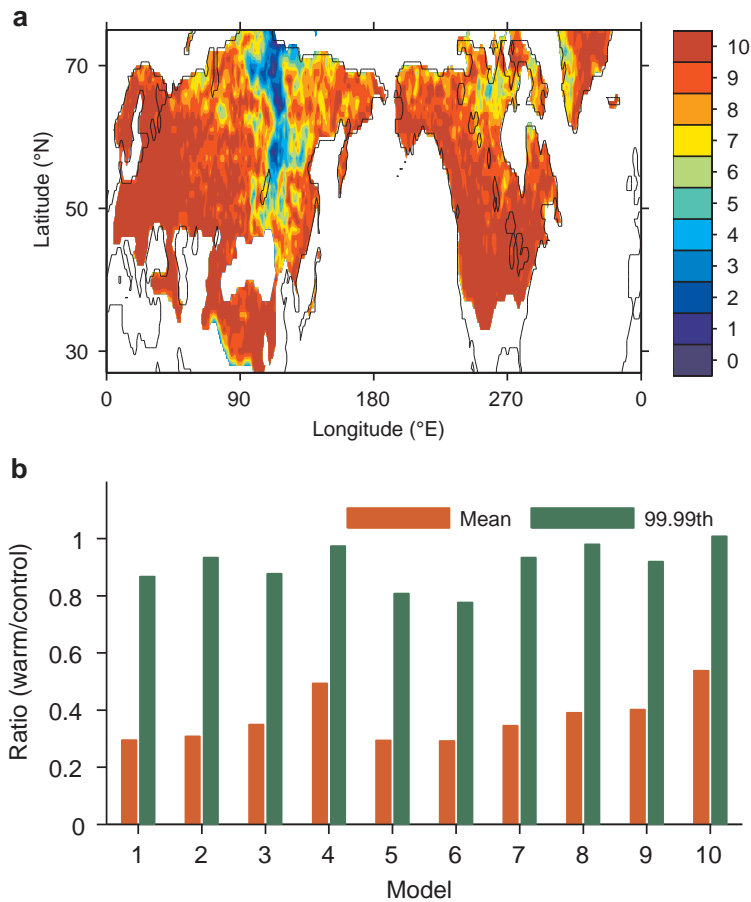
Extended Data Figure 3 | Mean and extreme snowfall as a function of climatological monthly surface air temperature in simulations and observations. a–d, The 99.99th (**a**), 99.9th (**b**), and 99th (**c**) percentiles of daily snowfall and mean snowfall (**d**) are shown for the control climate in the multimodel median (black solid line with circles; shading shows the interquartile range) and as estimated from GPCP/NCEP2 (black dashed line). CloudSat mean snowfall (red dashed-dotted line) is also shown in **d**. For the observational curves, NCEP2 monthly temperatures were used to define the climatological monthly surface air temperature bins. Only land grid boxes in the Northern Hemisphere (but all surface elevations) are included.

Extended Data Figure 4 | Mean and extreme snowfall in different climates as a function of climatological monthly surface air temperature. a–d, The multimodel-median 99.99th (**a**), 99.9th (**b**), and 99th (**c**) percentiles of daily snowfall and mean snowfall (**d**) are shown in the control climate (blue line with circles) and warm climate (red line with circles). The snowfall statistics shift left with warming (to some extent) because of the important influence of temperature on snowfall. Also shown are theoretical estimates given by equation (1) for high percentiles of snowfall in the control climate (blue dashed line) and the warm climate (red dashed line). Only land grid boxes in the Northern Hemisphere with surface elevation below 1,000 m are included.

Extended Data Figure 5 | Robustness of greater declines in mean snowfall compared with snowfall extremes in ten models from different centres (see Methods). a, Number of models out of ten in which the fractional decrease in the 20-year return value is less than that for mean snowfall or the 20-year return value increases. **b**, Ratios of mean snowfall (red) and the 99.99th percentile of daily snowfall (green) for the warm climate compared to the control climate and the −2.5 °C control-climate temperature bin. In **a**, only land grid boxes with mean snowfall greater than 5 cm per year in the control climate in the multimodel median are shown. In **b**, only Northern-Hemisphere land grid boxes with surface elevation below 1,000 m are included, and the models are identified by number in the 'Simulations' section of the Methods.
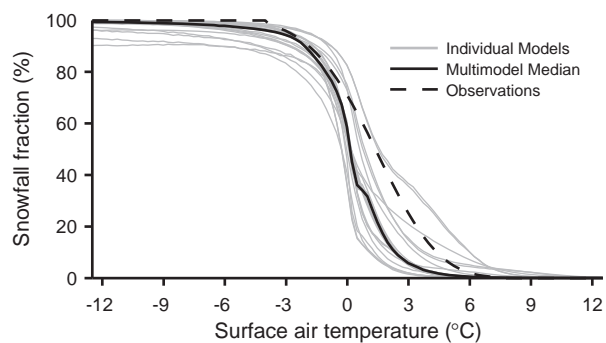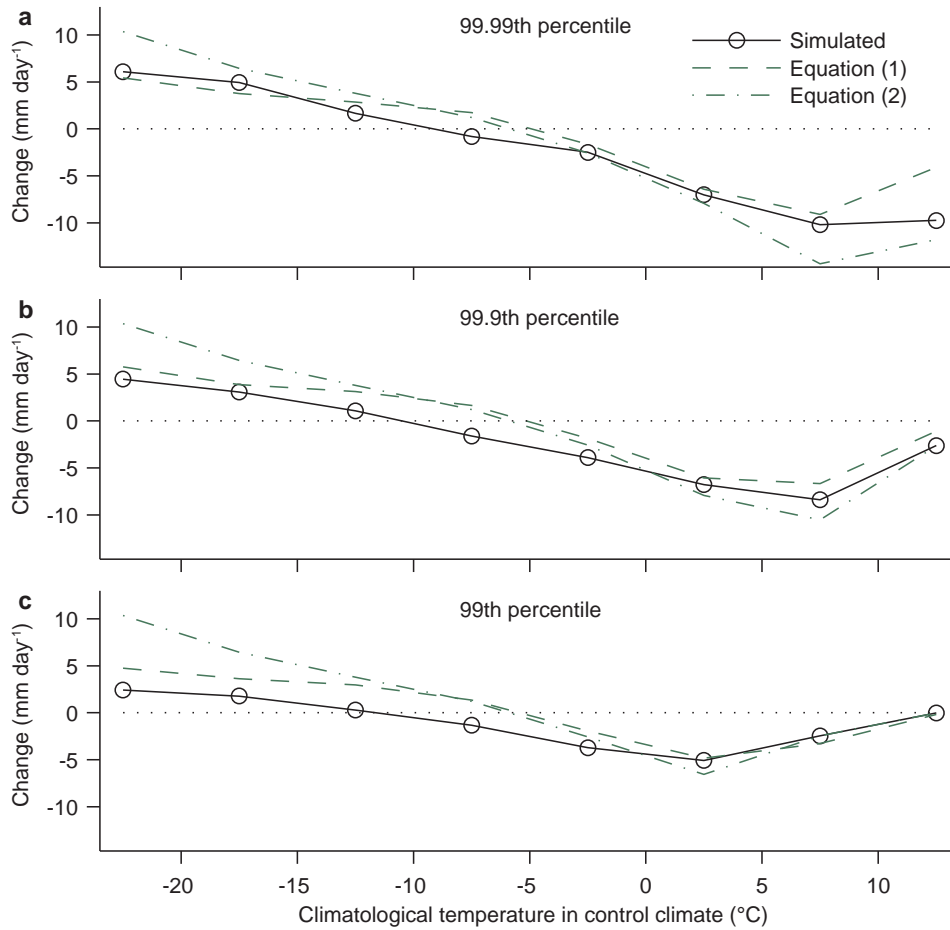
Extended Data Figure 6 | Snowfall fraction as a function of surface air temperature in simulations and observations. The snowfall fraction is shown for the control climate in individual models (grey lines) and the multimodel median (solid black line). A functional fit to observations is shown for comparison (black dashed line). The snowfall fraction for models is calculated as the ratio of mean snowfall to mean precipitation in daily temperature bins of width 0.25 °C, as in Fig. 3 but with all surface elevations included. The functional fit to the observed snowfall fraction is for three-hourly observations from Swedish meteorological stations[22].

a

← Snow   Rain →

Joint PDF

T_m $0°\text{C}$ T

b

Joint PDF

Control
Warm

0 s_q s_q $\hat{p}/h_m$
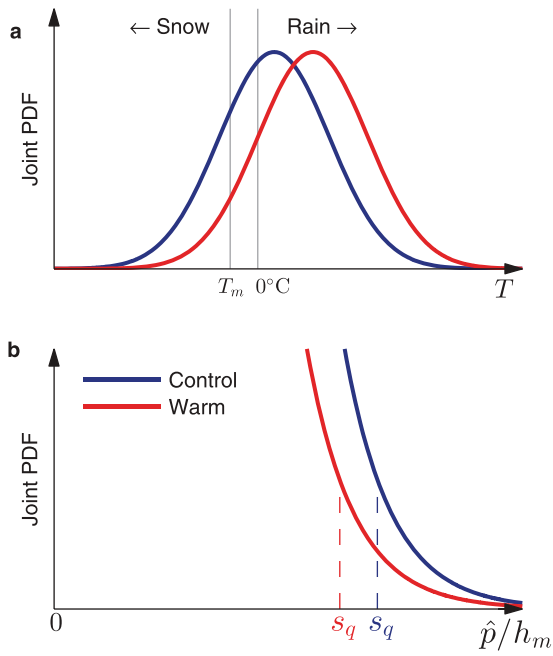
Extended Data Figure 7 | Schematic illustrating the effect of climate warming on the joint PDF of temperature T and normalized precipitation rate $\hat{p}$, and the resulting change in a high snowfall percentile s_q. a, b, The joint PDF as a function of T at a fixed $\hat{p}$ (**a**), and as a function of snowfall rate $\hat{p}/h_\mathrm{m}$ at $T = T_\mathrm{m}$ close to which snowfall extremes tend to occur (**b**). The joint PDF is shown for the control (blue) and warm (red) climates. Mean snowfall and the probability of snowfall can be inferred to decrease markedly with warming from **a**, while in **b** the area under the joint PDF to the right of s_q is the same in each climate, and s_q experiences a relatively small fractional decrease with warming.
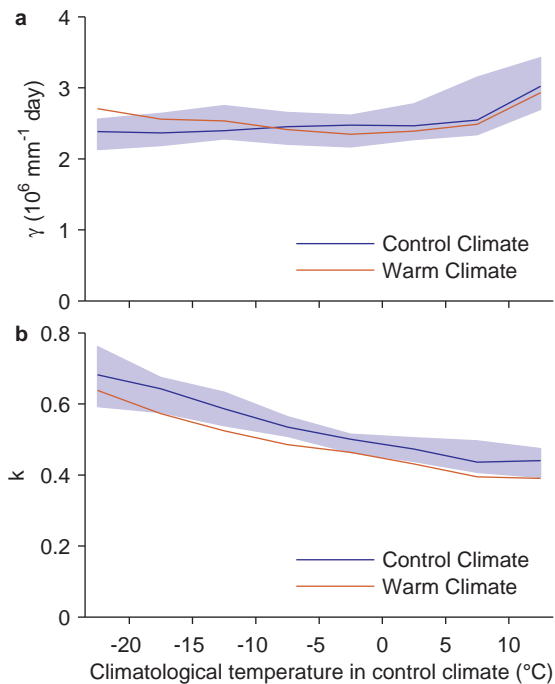
Extended Data Figure 8 | Parameters in the theory as a function of climatological monthly surface air in the control climate. a, b, Shown are the multimodel-medians of the rate parameter γ (**a**) and shape parameter k (**b**) in the control climate (blue line; shading shows the interquartile range) and warm climate (red line). Only land grid boxes in the Northern Hemisphere with surface elevation below 1,000 m are included.

Extended Data Figure 9 | Multimodel-median changes in snowfall extremes between the control and warm climates as a function of climatological monthly surface air temperature in the control climate. a–c, 99.99th (**a**), 99.9th (**b**) and 99th (**c**) percentiles of daily snowfall for the simulations (black line with circles), theory estimate from equation (1) (green dashed line), and simple theory estimate from equation (2) (green dashed-dotted line). The simple theory estimate is not independent of percentile for high climatological temperatures because it is constrained to not imply a negative snowfall rate in the warm climate. Only land grid boxes in the Northern Hemisphere with surface elevation below 1,000 m are included.
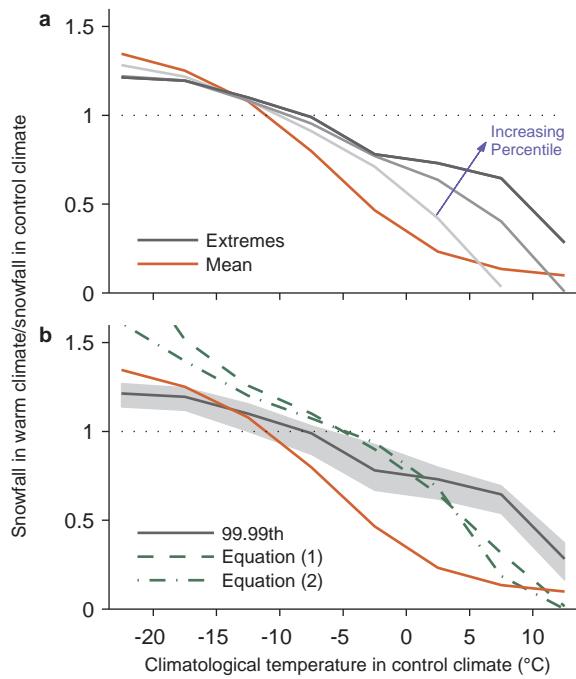
Extended Data Figure 10 | Ratios of snowfall for land grid boxes in the Northern Hemisphere with elevations at or above 1,000 m. a, b, Ratios are shown for the warm climate compared with the control climate as a function of climatological monthly surface air temperature in the control climate. Multimodel-median ratios of mean snowfall (red line) are shown in both panels. **a,** Multimodel-median ratios of the 99th, 99.9th and 99.99th percentiles of daily snowfall in increasing order from light to dark grey. **b,** Multimodel-median ratio of the 99.99th percentile of daily snowfall (grey line; shading shows the interquartile range), and the same ratio according to the theory estimate from equation (1) (green dashed line) and the simple theory estimate from equation (2) (green dashed-dotted line).